# EVALUATION OF ANALYTICAL PROCEDURES FOR PREDICTION OF TURBULENT BOUNDARY LAYERS ON A POROUS WALL

*by Charles E. Towne*

*Lewis Research Center*

*Cleveland, Ohio 44135*

| 1. Report No. NASA TM X-3063 | 2. Government Accession No. | 3. Recipient's Catalog No. |
|---|---|---|
| 4. Title and Subtitle EVALUATION OF ANALYTICAL PROCEDURES FOR PREDICTION OF TURBULENT BOUNDARY LAYERS ON A POROUS WALL | | 5. Report Date JUNE 1974 |
| | | 6. Performing Organization Code |
| 7. Author(s) Charles E. Towne | | 8. Performing Organization Report No. E-7635 |
| 9. Performing Organization Name and Address Lewis Research Center National Aeronautics and Space Administration Cleveland, Ohio 44135 | | 10. Work Unit No. 501-24 |
| | | 11. Contract or Grant No. |
| 12. Sponsoring Agency Name and Address National Aeronautics and Space Administration Washington, D.C. 20546 | | 13. Type of Report and Period Covered Technical Memorandum |
| | | 14. Sponsoring Agency Code |

15. Supplementary Notes·

16. Abstract

An analytical study has been made to determine how well current boundary layer prediction techniques work when there is mass transfer normal to the wall  The data that were considered in this investigation were for two-dimensional, incompressible, turbulent boundary layers with suction and blowing. Some of the bleed data were taken in an adverse pressure gradient. An integral prediction method was used with three different porous wall skin friction relations, in addition to a solid-surface relation, for the suction cases. A numerical prediction method was also used. Comparisons were made between theoretical and experimental skin friction coefficients, displacement and momentum thicknesses, and velocity profiles. The integral method with one of the porous wall skin friction laws gave very good agreement with data for most of the cases considered. The use of the solid-surface skin friction law caused the integral method to overpredict the effectiveness of the bleed. The numerical techniques also worked well for most of the cases.

| 17. Key Words (Suggested by Author(s)) Turbulent boundary layer Suction Injection Boundary layer analysis | 18. Distribution Statement Unclassified - unlimited Category 12 | | |
|---|---|---|---|
| 19. Security Classif. (of this report) Unclassified | 20. Security Classif. (of this page) Unclassified | 21. No. of Pages 31 | 22. Price* $3.25 |

*For sale by the National Technical Information Service, Springfield, Virginia 22151

# EVALUATION OF ANALYTICAL PROCEDURES FOR PREDICTION

# OF TURBULENT BOUNDARY LAYERS ON A POROUS WALL

## by Charles E. Towne

## Lewis Research Center

## SUMMARY

An analytical study has been made to determine how well current boundary layer prediction techniques work when there is mass transfer normal to the wall. The data that were considered in this investigation were for two-dimensional, incompressible, turbulent boundary layers with suction and blowing. Some of the bleed data were taken in an adverse pressure gradient. An integral prediction method was used with three different porous wall skin friction relations, in addition to a solid-surface relation, for the suction cases. A numerical prediction method was also used. Comparisons were made between theoretical and experimental skin friction coefficients, displacement and momentum thicknesses, and velocity profiles. The integral method with one of the porous wall skin friction laws gave very good agreement with data for most of the cases considered. The use of the solid-surface skin friction law caused the integral method to overpredict the effectiveness of the bleed. The numerical technique also worked well for most of the cases.

## INTRODUCTION

There are many situations where turbulent boundary layer prediction techniques must account for mass transfer normal to the wall. One of these is transpiration cooling, which involves blowing into the boundary layer. Another is boundary layer control in adverse pressure gradients by means of suction. This latter case is particularly applicable to flow in supersonic inlets, where bleed is often necessary to prevent separation (refs. 1 and 2). It is not difficult to include the terms involving mass flux normal to the wall in the boundary layer equations, but little attempt has been made to systematically compare how well current prediction techniques work under these conditions.

This report, therefore, presents the results of two analytical procedures, along with data, for several turbulent boundary layers on a porous wall. The integral method is that of Sasman and Cresci (ref. 3), modified to include the terms involving the velocity normal to the wall. With integral procedures, a modification to the usual solid-surface skin friction relation to account directly for nonzero velocities at the wall is also necessary. Three different skin friction laws (refs. 4 to 6), applicable to boundary layers with suction, are used in the integral analysis. The numerical method of McDonald and Fish (ref. 7) is used to verify the integral results and is also used with some injection cases. Comparisons are made between theoretical and experimental displacement thickness, momentum thickness, and skin friction coefficient. Velocity profiles are also presented for the numerical method.

Analytical methods require knowledge of the mass flow distribution normal to the wall through the bleed or blowing region. Because of a lack of data of this type for compressible flow, the data considered in this report are for incompressible, two-dimensional flow. Several different mass transfer rates and distributions are investigated. Some of the data that are used were taken in a pressure gradient.

## SYMBOLS

A $\quad$ function of $\text{Re}_\theta$ (see eq. (2))

B $\quad$ function of $\text{Re}_\theta$ (see eq. (2))

$C_f$ $\quad$ skin friction coefficient

$C_{f_o}$ $\quad$ skin friction coefficient with $v_w = 0$

H $\quad$ shape factor, $\delta^*/\theta$

h $\quad$ enthalpy

j $\quad$ dimensionality parameter

$l_\infty$ $\quad$ "wake" value of mixing length

M $\quad$ Mach number

Pr $\quad$ laminar Prandtl number

p $\quad$ pressure

R $\quad$ radius of axisymmetric body

$\text{Re}_x$ $\quad$ Reynolds number based on $x$

$\text{Re}_\theta$ $\quad$ Reynolds number based on $\theta$

T $\quad$ temperature

U     transformed x-velocity

u     x-velocity

V     transformed y-velocity

v     y-velocity

X     transformed x-coordinate

x     coordinate along body surface

Y     transformed y-coordinate

y     coordinate normal to body surface

z     $\ln Re_{\theta}$

$\gamma$     ratio of specific heats

$\Delta$     transformed boundary layer thickness

$\delta$     boundary layer thickness

$\delta^*$     displacement thickness, $\displaystyle\int_0^{\delta}\left(1 - \frac{\rho u}{\rho_e u_e}\right)dy$

$\theta$     momentum thickness, $\displaystyle\int_0^{\delta}\frac{\rho u}{\rho_e u_e}\left(1 - \frac{u}{u_e}\right)dy$

$\mu$     viscosity coefficient

$\nu$     kinematic viscosity coefficient

$\rho$     density

$\tau$     shear stress

Subscripts:

e     local external conditions

i     transformed value

s     local stagnation conditions

w     conditions at wall

0     free stream stagnation conditions

Superscript:

‾     evaluated at reference conditions (see eq. (A5))

# METHOD OF ANALYSIS

Two analytical techniques, one numerical and one integral, were used in this investigation. The integral method that was used is essentially that of Sasman and Cresci (ref. 3). This method uses the transformed momentum and moment of momentum integral equations, requiring starting values of momentum and displacement thicknesses. The equations are coupled and solved simultaneously by a Runge-Kutta integration routine. For this study the equations were modified to include terms involving the velocity normal to the wall and to allow the use of different skin friction relations. The details of this modification are given in the appendix.

The skin friction relation used in reference 3 is

$$C_f = 0.246 \, e^{-1.561 \, H_i} \left(\frac{U_e \theta_i}{\nu_0}\right)^{-0.268} \frac{T_e}{\overline{T}} \left(\frac{\overline{\mu}}{\mu_0}\right)^{0.268} \tag{1}$$

Using this solid-surface relation in a prediction method with suction will lead to inaccurate predictions of the boundary layer growth, as pointed out in reference 4. It is therefore necessary to use a skin friction equation that directly accounts for the velocity normal to the wall.

Three different relations of this type were tried. The first was from Thompson (ref. 4). It is based on a three-parameter family of velocity profiles, and is applicable to incompressible flows with small adverse pressure gradients. This relation is presented both graphically and as an analytic approximation by Krishnamurthy in reference 4. The analytic approximation was used in this study, and is of the form

$$C_f = e^{AH+B} \tag{2}$$

Letting $z = \ln Re_\theta$, for $v_w/u_e = 0$ the values of $A$ and $B$ are given by

$$A = 0.019521 - z[0.386768 - z(0.028345 - 0.0007017z)],$$

$$B = 0.191511 - z[0.834891 - z(0.062588 - 0.001953z)]$$

For $v_w/u_e = -0.005$

$$A = 1.07085 - z[0.831747 - z(0.106843 - 0.004428z)],$$

$$B = -2.338049 + z[0.015834 - z(0.047968 - 0.003308z)]$$

For $v_w/u_e = -0.010$

$$A = -1.00747 - e^{(10.97531 - 8.1080555 \ln z)}$$

$$B = 110.92\ e^{-1.06z} - 2.94$$

The value of $C_f$ at a given $v_w/u_e$ was found by linear interpolation or extrapolation using these values.

The other two skin friction relations that were used are based on incompressible flat plate data. Both depend on $C_{fo}$, the value of the skin friction coefficient without bleed. One of these equations (ref. 5) is

$$C_f = \frac{-1.62\ \dfrac{\rho_w v_w}{\rho_e u_e}}{1 - e^{\left(-\dfrac{1.62}{C_{fo}}\dfrac{\rho_w v_w}{\rho_e u_e}\right)}}$$

The other, from reference 6, is

$$C_f = C_{fo}\ e^{-0.748\ \frac{\rho_w v_w}{\rho_e u_e}\frac{1}{C_{fo}}}$$

For these equations the value of $C_{fo}$ was found by using the Sasman-Cresci method with equation (1).

The numerical method is that of McDonald and Fish (ref. 7). It is based on a mixing length turbulence model and uses a general implicit finite-difference scheme to solve the boundary layer equations. In reference 7 it is stated that the value of the outer layer normalized mixing length, $l_\infty/\delta$, is allowed to vary in the streamwise direction for non-equilibrium boundary layers, requiring the use of the integral turbulence kinetic energy equation. For this investigation, however, $l_\infty/\delta$ was set at a constant value of 0.09. A correction to the turbulence model for low Reynolds number flows, given in reference 8, was included in the analysis.

The numerical method requires starting velocity and temperature profiles. Several different techniques can be used to obtain these profiles. The experimental profiles can be used, if available, or they can be found by using the flat plate turbulent boundary layer profile family of Maise and McDonald (ref. 9). In addition, an "equilibrium" start

can be used in which an iteration upon the starting profiles is performed. This method tends to relax and improve a poor guess for the starting profiles, and was used for all cases in this study.


## RESULTS AND DISCUSSION

### Zero Pressure Gradient

The zero pressure gradient data that were used are those of Simpson (ref. 10). These data were taken on a flat plate with a smooth porous surface of sintered bronze. The porous region was 45.7 centimeters wide and 244 centimeters long. A boundary layer trip was located 0.318 centimeter upstream of the start of the porous surface. Boundary layer profiles were measured along the plate centerline at various distances from the leading edge. Table I presents the free stream conditions and bleed rates for the Simpson cases used in this study. Some of the mass transfer rates are functions of x, the distance along the plate from the start of the porous region. The run numbers correspond to those of reference 10.

The zero pressure gradient bleed cases were analyzed using the integral method of reference 3 with four different skin friction laws. The starting values of displacement and momentum thickness were those that gave good agreement at the first experimental probe location for the zero mass transfer case (run 31067). The theoretical values of the skin friction coefficient for run 31067 were used for $C_{f_o}$ in the correlations of references 5 and 6.

The results are shown in figure 1. The use of the solid-surface skin friction relation of reference 3 tended to overpredict the bleed effectiveness. The skin friction laws of references 5 and 6, based on flat plate data, gave somewhat better results, but the best results were obtained by using the curve fit to the skin friction law of reference 4. An exception was the high bleed case shown with an expanded scale in figure 1(b). Here the experimental momentum and displacement thicknesses were close to their laminar asymptotic values of 0.012 and 0.025 centimeters (ref. 11). This may indicate that the boundary layer flow is becoming laminar due to the large bleed rate. Under these conditions it is difficult to say which skin friction relation gave the best agreement. When the correlation of reference 5 was used for this case, the integral thicknesses went to zero because the bleed terms in the governing equations became dominant.

All 11 of the zero pressure gradient cases were analyzed using the numerical prediction technique. The starting value of displacement thickness for all cases was the same as that used with the integral method. The initial profiles were found from reference 9 as previously discussed.

6

Figure 2 compares theoretical and experimental values of skin friction coefficient, momentum thickness, and displacement thickness. The configurations with uniform blowing and bleed are presented in figures 2(a) and (b), those with variable mass transfer rates in figures 2(c) and (d), and those with step changes in the mass transfer rate in 2(e) and (f). The results for the no mass transfer case are shown on each plot as a reference. Excellent agreement was obtained for all configurations. Velocity profiles are presented in figure 3 for five of these cases. Again excellent agreement was obtained.

## Nonzero Pressure Gradient

The adverse pressure gradient bleed data were taken on the flat part of the upper surface of a symmetrical airfoil by Thompson (ref. 12). The airfoil had a chord length of 81.2 centimeters and a circular leading edge of radius 8.25 centimeters. The suction surface itself was 54.6 centimeters long and made of a smooth porous plastic material. Boundary layer profiles were measured at seven stations along the airfoil, with the first just upstream of the start of the suction surface. In addition, static pressure taps were located along the surface to determine the external velocity distribution.

Five different boundary layers were analyzed, identified as layers B, D, F, G, and H in reference 12. Layers B and D were measured with the airfoil at an angle of attack of $-6^O$ for layer B and $+5^O$ for layer D. For layers F, G, and H, a leading edge section was attached, and the airfoil was used as a flap, at a flap angle of approximately $17^O$. Figure 4 shows the experimentally determined external velocity distributions and figure 5 the bleed flow distributions for the five cases that were studied. These experimental values were those used for the analysis.

The results of the integral analysis of reference 3 were compared with the adverse pressure gradient data. The experimental momentum and displacement thicknesses just upstream of the bleed region were used as starting values. The method was first used without bleed to determine the values of $C_{fo}$ for the skin friction correlations of references 5 and 6. The results are shown in figure 6. Note that layers F, G, and H appear close to separation without bleed.

Figure 7 compares the results of the integral method using the various skin friction relations with the adverse pressure gradient data. For all cases, the solid-surface skin friction relation overpredicts the effectiveness of the bleed, and to a greater degree than for the zero pressure gradient cases previously discussed. The relation of reference 4 generally gave very good agreement with the data. The correlations of references 5 and 6 gave poor results. This should be expected, since these correlations are based on zero pressure gradient data.

For layer B, the momentum and displacement thicknesses, shown on an expanded scale in figure 7(a), went to zero because of the high bleed rate when the skin friction laws of references 3 to 5 were used. The correlation of reference 6 gave too high a value for $C_f$, causing the method to blow up just downstream of the start of suction, and is not shown in figure 7(a). The correlations of references 5 and 6 both caused the method to eventually blow up for the remaining cases also.

For the numerical technique, the experimental velocity profile just upstream of the bleed region was used to start the calculations. The starting temperature profile was determined by assuming a Crocco temperature distribution. The equilibrium starting method was used, as previously discussed.

Figure 8 compares the results of the numerical technique with the experimental values of momentum and displacement thickness. The theoretical skin friction coefficient is also shown, but no experimental skin friction measurements were made. Good agreement was obtained for the three lower speed cases, layers B, D, and H. The agreement was not as good, however, for layers F and G. The same results were found for the velocity profiles, figure 9. There are several possible reasons for the disagreement found in layers F and G. Both of these cases involve a fairly strong adverse pressure gradient and a small bleed rate. There may be limitations in the mixing length model that was used in this study when applied under these conditions. Small errors in the experimental bleed rate may be important in an adverse pressure gradient. There was also a blockage effect due to the supporting structure beneath the porous surface that was not taken into account.

For a further evaluation of the numerical method of reference 7, two additional cases were considered, both involving injection in a pressure gradient. The data were taken by McQuaid (ref. 13) on a flat plate with a porous region 76.2 centimeters long. One of the cases, called pressure distribution I in reference 13, was for a slightly adverse pressure gradient. The other, pressure distribution II, was a favorable gradient. Boundary layer measurements were made with a pitot pressure probe at various stations along the plate. Static pressure taps were used to determine the streamwise velocity distributions.

These velocity distributions, along with the experimental injection rates, were used as input for the analysis. The values of the velocity were all of the order of 15 meters per second. The local injection rate $v_w/u_e$ was around 0.002 for pressure distribution I and 0.008 for pressure distribution II. The calculations were started at the first probe location by using the experimental displacement thickness. The boundary layer profiles were found by the method of reference 9, as previously discussed.

Figure 10 presents the theoretical and experimental values of momentum and displacement thickness for both pressure distributions. The predicted skin friction coefficient is also shown. The velocity profiles are given in figure 11. Excellent agreement was obtained for both cases.

# SUMMARY OF RESULTS

Comparisons of analysis and data have been made for turbulent boundary layers with suction and blowing normal to the wall. Two different prediction methods were used. In addition, three different porous wall skin friction relations were used with an integral method for comparisons with the suction cases. Results of a numerical technique are also presented. The data were for incompressible, two-dimensional flow with several different mass transfer rates and distributions. Pressure gradient effects were present in some of the data. Comparisons were made of theoretical and experimental skin friction coefficients, displacement and momentum thicknesses, and velocity profiles.

The results of the investigation can be summarized as follows:

1. In the zero pressure gradient cases, the integral theory gave better agreement with data when the porous wall skin friction relations were used in place of the solid-surface relation. One of the porous wall equations, intended for use in zero and mild pressure gradients, was consistently better than the others.

2. For the cases with pressure gradient, the two porous wall skin friction laws based on flat plate flows gave poor agreement with data. The third, applicable to cases with mild pressure gradient, gave good agreement for the low speed cases with high bleed rates, but slightly underestimated the displacement thickness for the cases with lower bleed rates.

3. The numerical technique gave excellent agreement with data for all the zero pressure gradient cases considered. Good agreement was also obtained for the four low speed adverse pressure gradient cases. The velocity profile predictions, however, were not as good for the two more severe pressure gradient cases.

In order to apply theory to boundary layers across bleed regions in supersonic inlets, more experimental work needs to be done in compressible flow and in adverse pressure gradients. Skin friction data is needed in addition to velocity profiles. Detailed measurements of the bleed mass flow distribution are also required.

Lewis Research Center,
   National Aeronautics and Space Administration,
      Cleveland, Ohio, March 6, 1974,
         501-24.

# APPENDIX – MODIFICATION OF SASMAN-CRESCI INTEGRAL EQUATIONS

For steady, compressible, turbulent flow the time averaged boundary layer equations are

$$\frac{\partial(\rho u)}{\partial x} + \frac{\partial(\rho v)}{\partial y} + j\,\frac{\rho u}{R}\,\frac{dR}{dx} = 0 \tag{A1}$$

$$\rho u\,\frac{\partial u}{\partial x} + \rho v\,\frac{\partial u}{\partial y} = -\frac{dp}{dx} + \frac{\partial \tau}{\partial y} \tag{A2}$$

where $j = 0$ for two-dimensional flow and 1 for axisymmetric flow.

These equations are transformed using the method of reference 3, given by

$$X = \int_0^x \left(\frac{T_0}{\overline{T}}\right)\left(\frac{T_e}{T_0}\right)^{(\gamma+1)/2(\gamma-1)} dx \tag{A3}$$

and

$$Y = \left(\frac{T_e}{T_0}\right)^{1/2} \int_0^y \frac{\rho}{\rho_0}\,dy \tag{A4}$$

where

$$\frac{\overline{T}}{T_0} = \frac{1}{2}\frac{T_w}{T_0} + 0.22\,Pr^{1/3} + (0.5 - 0.22\,Pr^{1/3})\,\frac{T_e}{T_0} \tag{A5}$$

The continuity equation (A1) becomes

$$\frac{\partial U}{\partial X} + \frac{\partial V}{\partial Y} + j\,\frac{U}{R}\,\frac{dR}{dX} = 0 \tag{A6}$$

and the momentum equation (A2) transforms to

$$U\,\frac{\partial U}{\partial X} + V\,\frac{\partial U}{\partial Y} = \frac{h_s}{h_0}\,U_e\,\frac{dU_e}{dX} + \frac{1}{\rho_e}\,\frac{\overline{T}}{T_e}\,\frac{\partial \tau}{\partial Y} \tag{A7}$$

Using equations (A6) and (A7) and following the procedure outlined in references 14 and 15, but without setting $V_w = 0$, gives the transformed momentum integral equation

$$\frac{d\theta_i}{dX} + \frac{\theta_i}{U_e}\frac{dU_e}{dX}\left[2 + H_i + \frac{1}{\theta_i}\int_0^\Delta \left(\frac{h_s}{h_0} - 1\right)dy\right] + j\frac{\theta_i}{R}\frac{dR}{dX} - \frac{V_w}{U_e} = \frac{T_0}{T_e}\frac{\bar{T}}{T_0}\frac{\tau_w}{\rho_e U_e^2} \qquad (A8)$$

and the transformed moment-of-momentum integral equation

$$\frac{dH_i}{dX} = -\frac{1}{U_e}\frac{dU_e}{dX}\left[\frac{H_i\left(H_i + 1\right)^2(H_i - 1)}{2}\right] \cdot$$

$$\left[1 + \frac{2}{\theta_i}\frac{1}{H_i + 1}\int_0^\Delta \left(\frac{h_s}{h_0} - 1\right)dy - \frac{2(H_i - 1)}{H_i^2(H_i + 1)\theta_i^2}\int_0^\Delta \left(\frac{h_s}{h_0} - 1\right)Y\,dY\right]$$

$$+ \frac{H_i\left(H_i^2 - 1\right)}{\theta_i}\frac{T_0}{T_e}\frac{\bar{T}}{T_0}\frac{\tau_w}{\rho_e U_e^2} - \frac{\left(H_i^2 - 1\right)(H_i + 1)}{\theta_i}\frac{T_0}{T_e}\frac{\bar{T}}{T_0}\frac{\tau_w}{\rho_e U_e^2}\int_0^1 \frac{\tau}{\tau_w}d\left(\frac{Y}{\Delta}\right) + \frac{\left(H_i^2 - 1\right)}{\theta_i}\frac{V_w}{U_e}$$

$$(A9)$$

Now following reference 3, these become

$$\frac{d\theta_i}{dx} = -\frac{\theta_i}{M_e}\frac{dM_e}{dx}\left(2 + \frac{T_w}{T_0}H_i\right) - j\frac{\theta_i}{R}\frac{dR}{dX} + \left[\frac{p_e}{p_0}\frac{T_0}{T_w}\left(\frac{T_e}{T_0}\right)^{1/2}\frac{v_w}{u_e} + \left(\frac{T_e}{T_0}\right)^{(\gamma+1)/2(\gamma-1)}\frac{C_f}{2}\right] \qquad (A10)$$

and

$$\frac{dH_i}{dx} = -\frac{1}{2M_e}\frac{dM_e}{dx}\left[H_i\left(H_i+1\right)^2(H_i-1)\right]\left[1+\left(\frac{T_w}{T_0}-1\right)\frac{H_i^2+4H_i-1}{(H_i+1)(H_i+3)}\right]$$

$$-\frac{0.011}{\theta_i}(H_i+1)\left(H_i^2-1\right)\left(\frac{H_i-1}{H_i}\right)^2\frac{T_0}{\bar{T}}\left(\frac{T_e}{T_0}\right)^{(\gamma+1)/2(\gamma-1)}$$

$$+\frac{\left(H_i^2-1\right)H_i}{\theta_i}\left(\frac{T_e}{T_0}\right)^{(\gamma+1)/2(\gamma-1)}\frac{C_f}{2}+\frac{H_i^2-1}{\theta_i}\frac{p_e}{p_0}\frac{T_0}{T_w}\left(\frac{T_e}{T_0}\right)^{1/2}\frac{v_w}{u_e} \quad \text{(A11)}$$

These equations are in a slightly different form than those of reference 3. The momentum integral equation has been left in terms of $\theta_i$, and $h_w/h_0$ has been replaced by $T_w/T_0$. The skin friction coefficient appears explicitly in equations (A7) and (A8), allowing the use of different equations for $C_f$ when $v_w$ is nonzero. The relation between $v_w$ and $V_w$ is given by

$$\frac{V_w}{U_e} = \frac{\bar{T}}{T_e}\frac{T_0}{T_w}\frac{v_w}{u_e} \quad \text{(A12)}$$

# REFERENCES

1. Cubbison, Robert W.; Meleason, Edward T.; and Johnson, David F.: Effect of Porous Bleed in a High-Performance Axisymmetric, Mixed-Compression Inlet at Mach 2.50. NASA TM X-1692, 1968.

2. Hingst, Warren R.; and Johnson, David F.: Experimental Investigation of Boundary Layers in an Axisymmetric, Mach 2.5, Mixed Compression Inlet. NASA TM X-2902, 1973.

3. Sasman, Philip K.; and Cresci, Robert J.: Compressible Turbulent Boundary Layer with Pressure Gradient and Heat Transfer. AIAA Jour., vol. 4, no. 1, Jan. 1966, pp. 19-25.

4. Thompson, B. G. J.: A Three-Parameter Family of Mean Velocity Profiles for Incompressible Turbulent Boundary Layers with Distributed Suction and Small Pressure Gradient. R. & M. 3622, British ARC, 1970.

5. Verollet, E.; Fulachier, L.; Dumas, R.; and Favre, A.: Turbulent Boundary Layer with Suction and Heating to the Wall. In: Heat and Mass Transfer in Turbulent Boundary Layers, Vol. 1. N. Afgan, Z. Zaric, and P. Anastasyevic, eds., Pergamon Press, 1972, pp. 157-168.

6. Arie, M. Ia.: Turbulent Boundary Layer on a Porous Surface. Gidromekhanika, no. 15, 1969, pp. 55-59.

7. McDonald, Henry; and Fish, R. W.: Practical Calculations of Transitional Boundary Layers. Int. Jour. Heat and Mass Transfer, vol. 16, no. 9, Sept. 1973, pp. 1729-1744.

8. McDonald, Harry: Mixing Length and Kinematic Eddy Viscosity in a Low Reynolds Number Boundary Layer. Rept. J214453-1, United Aircraft Research Laboratories, Sept. 1970.

9. Maise, George; and McDonald, Henry: Mixing Length and Kinematic Eddy Viscosity in a Compressible Boundary Layer. AIAA Jour., vol. 6, no. 1, Jan. 1968, pp. 73-80.

10. Simpson, Roger Lyndon: The Turbulent Boundary Layer on a Porous Plate: An Experimental Study of the Fluid Dynamics with Injection and Suction. Ph. D. Thesis, Stanford Univ., 1968.

11. Schlichting, Herman: Boundary-Layer Theory. 6th ed., McGraw Hill Book Co., Inc., 1968, p. 369.

12. Thompson, B. G. J.: An Experimental Investigation into the Behavior of the Turbulent Boundary Layer with Distributed Suction in Regions of Adverse Pressure Gradient. R. & M. 3621, British ARC, 1970.

13. McQuaid, J.: Experiments on Incompressible Turbulent Boundary Layers with Distributed Injection. R. & M. 3549, British ARC, 1968.

14. Reshotko, Eli; and Tucker, Maurice: Approximate Calculation of the Compressible Turbulent Boundary Layer with Heat Transfer and Arbitrary Pressure Gradient. NACA TN 4154, 1957.

15. Tetervin, Neal; and Lin, Chia Chiao: A General Integral Form of the Boundary-Layer Equation for Incompressible Flow with an Application to the Calculation of the Separation Point of Turbulent Boundary Layers. NACA TR-1046, 1951. (Supersedes NACA TN 2158.)

TABLE I. - FREE STREAM CONDITIONS AND BLEED RATES

FOR SIMPSON DATA (REF. 10)

| Run number | Velocity $u_e$, m/sec | Temperature $T_e$, K | Pressure $p_e$, N/m$^2$ | Bleed or injection rate, $v_w/u_e$ |
|---|---|---|---|---|
| 31 067 | 12. 85 | 292. 2 | 100 900 | 0 |
| 122 866 | 14. 04 | 304. 1 | 102 500 | +0.00099 |
| 122 066 | 14. 10 | 304. 7 | 101 200 | +0.0038 |
| 21 067 | 12. 96 | 291. 4 | 101 600 | -0.0012 |
| 2 867 | 13. 02 | 291. 0 | 102 200 | -0.0046 |
| 12 467 | 13. 12 | 289. 9 | 100 200 | $-0.056 \ Re_x^{-1/5}/u_e$ |
| 3 867 | 12. 80 | 291. 6 | 100 900 | $+0.101 \ Re_x^{-1/5}/u_e$ |
| 61 367 | 12. 83 | 293. 7 | 100 500 | $+5.0 \times 10^{-5} \ x$ |
| 42 567 | 13. 18 | 291. 8 | 102 200 | $\begin{cases} 0.0 \text{ for } Re_x < 8.14 \times 10^5 \\ +0.001 \text{ for } Re_x > 8.14 \times 10^5 \end{cases}$ |
| 5 167 | 13. 26 | 292. 6 | 102 000 | $\begin{cases} 0.0 \text{ for } Re_x < 8.15 \times 10^5 \\ +0.0039 \text{ for } Re_x > 8.15 \times 10^5 \end{cases}$ |
| 62 367 | 13. 12 | 294. 6 | 100 700 | $\begin{cases} -0.0024 \text{ for } Re_x < 7.95 \times 10^5 \\ 0.0 \text{ for } Re_x > 7.95 \times 10^5 \end{cases}$ |

(a) Run 21067; $v_w/u_e = -0.0012$.

(b) Run 2867; $v_w/u_e = -0.0046$.
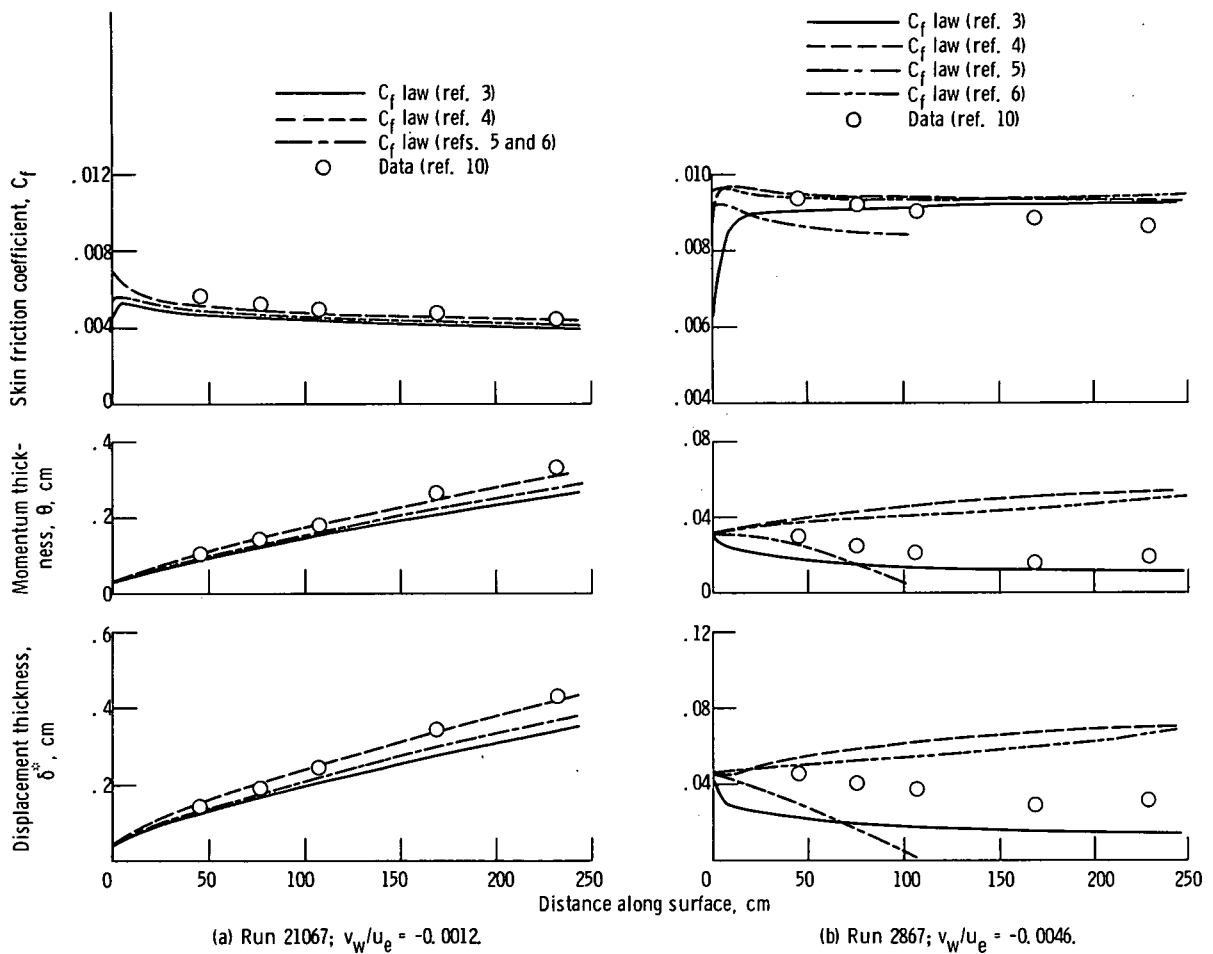
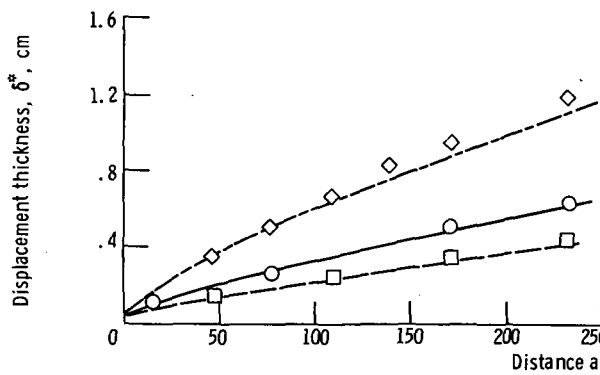Figure 1. - Effect of skin friction law on turbulent boundary layer analysis for Simpson flat plate.

Cf law (ref. 3)
Cf law (ref. 4)
Cf law (refs. 5 and 6)
○    Data (ref. 10)

Skin friction coefficient, $C_f$

.008

.004

0

Momentum thickness, $\theta$, cm

.4

.2

0

Displacement thickness, $\delta^*$, cm

.6

.4

.2

0        50       100      150      200      250

Distance along surface, cm

(c) Run 12467; $v_w/u_e = -0.056 \, Re_x^{-1/5}/u_e$.

(d) Run 62367; step in suction rate at $x = 92$ centimeters from $v_w/u_e = -0.0024$ to 0.0.

Figure 1. - Concluded.

17 ·

(a) For uniform blowing.

(b) For uniform suction.
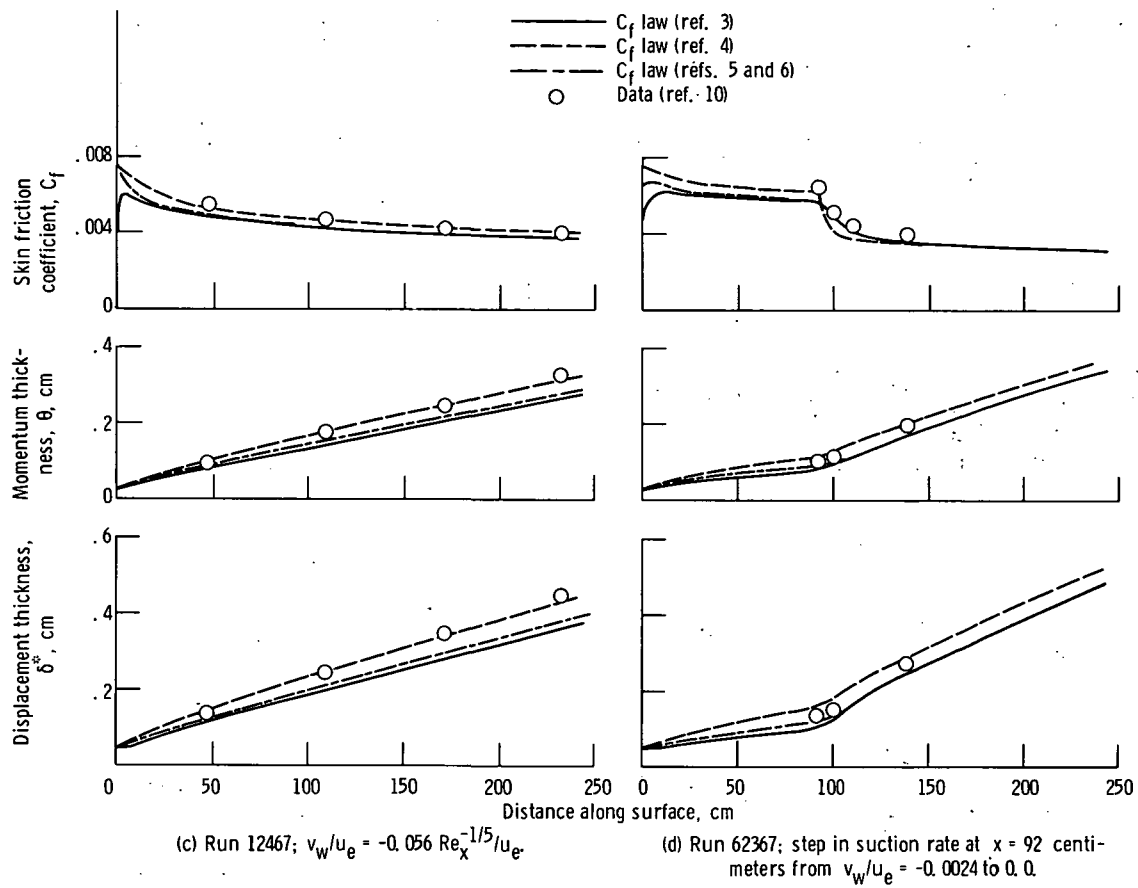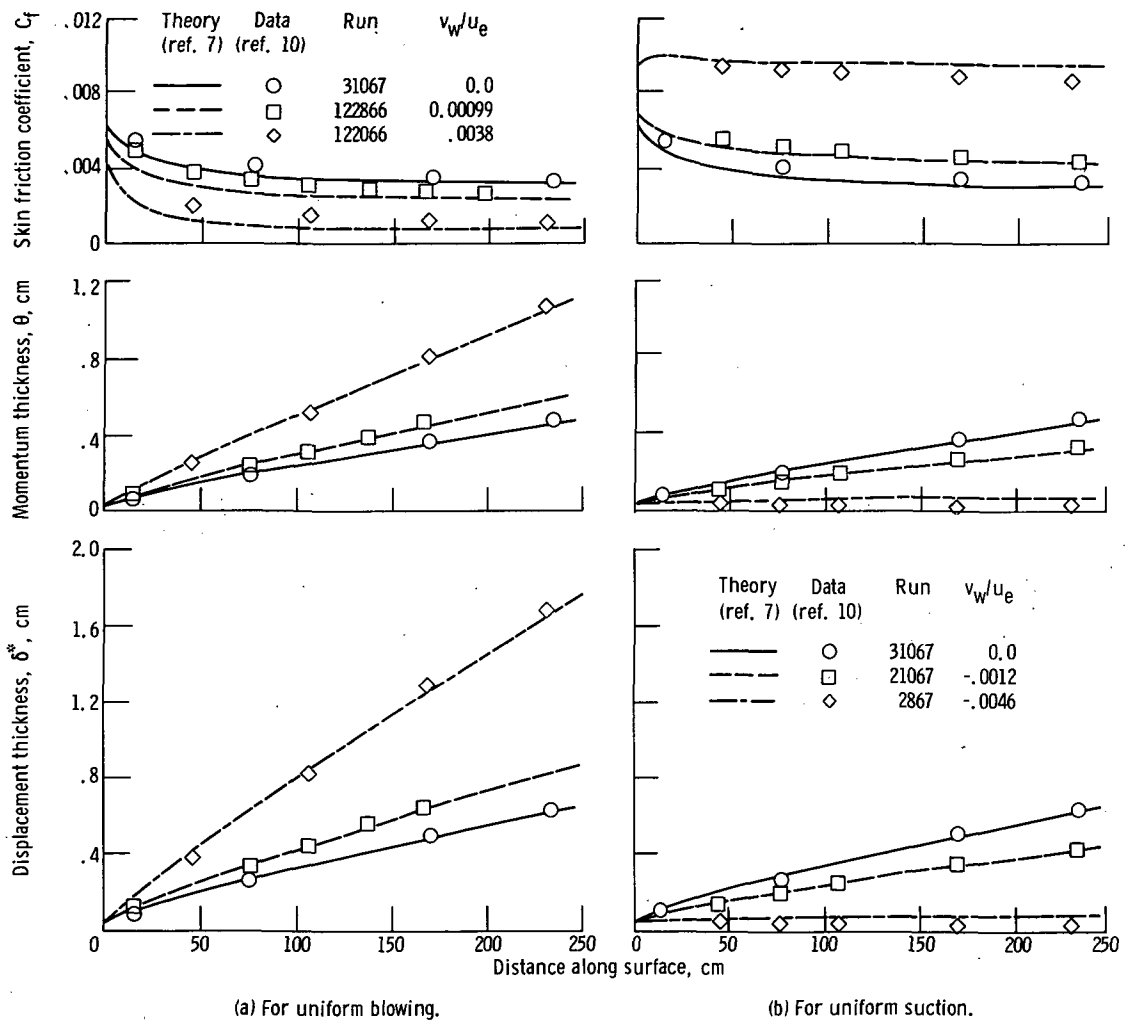
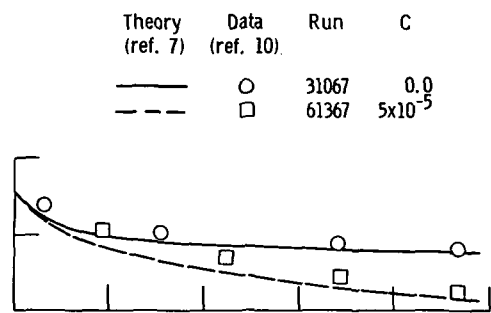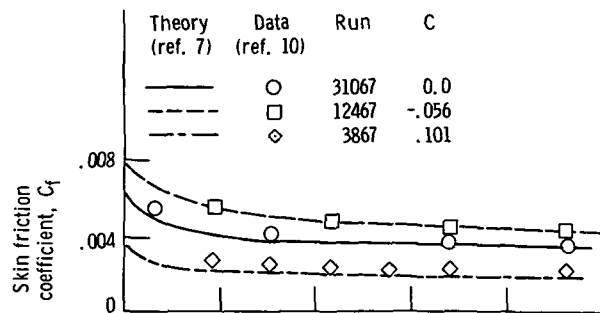Figure 2. - Theoretical and experimental results for Simpson flat plate.
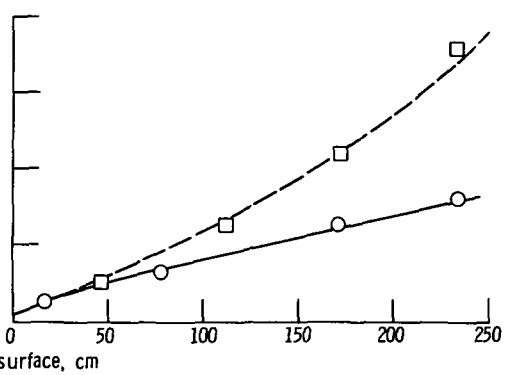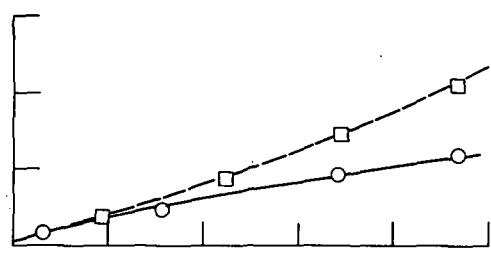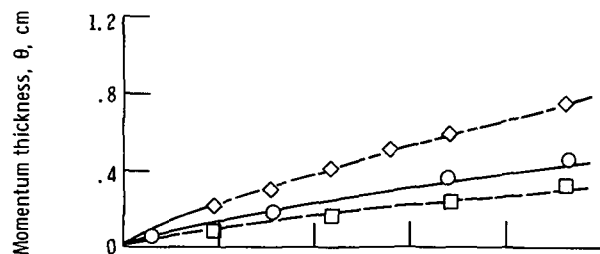
(c) For $v_w/u_e = C Re_x^{-1/5}/u_e$.
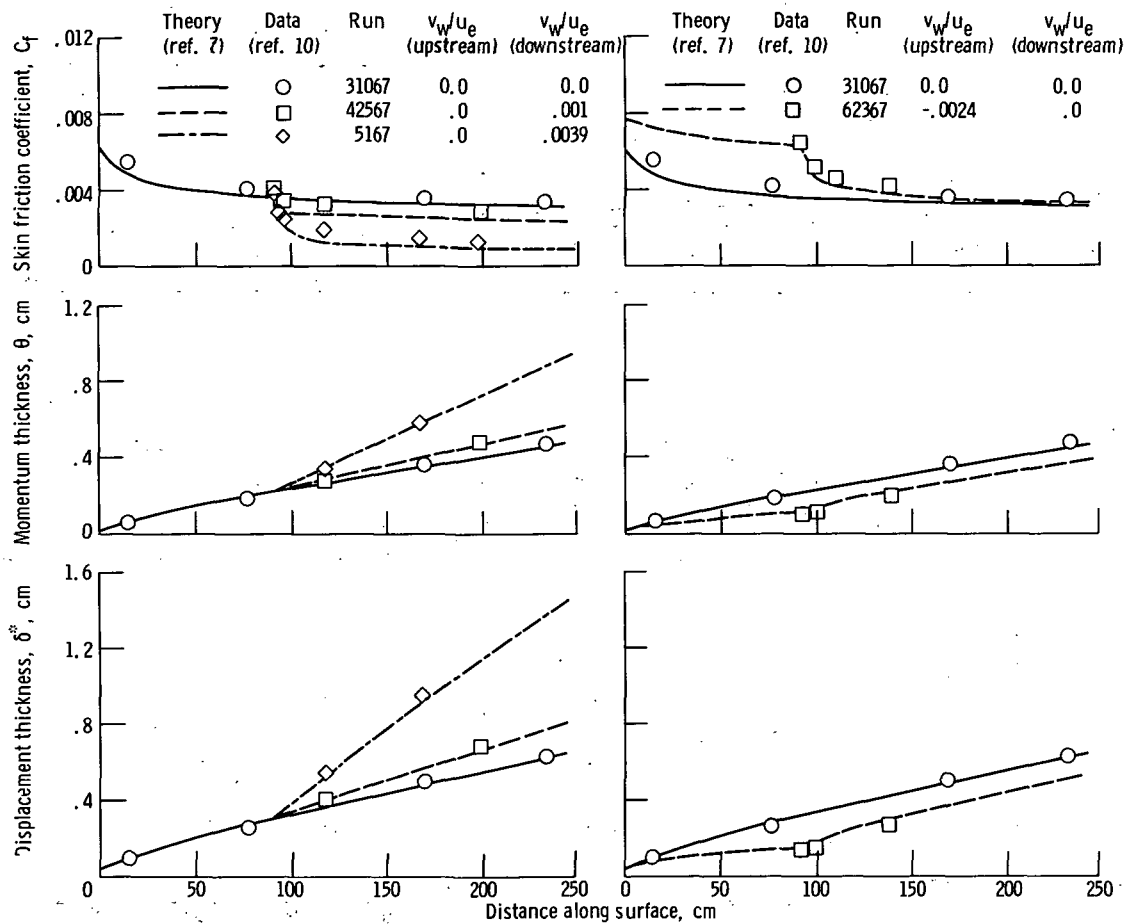
(d) For $v_w/u_e = Cx$.

Figure 2. - Continued.

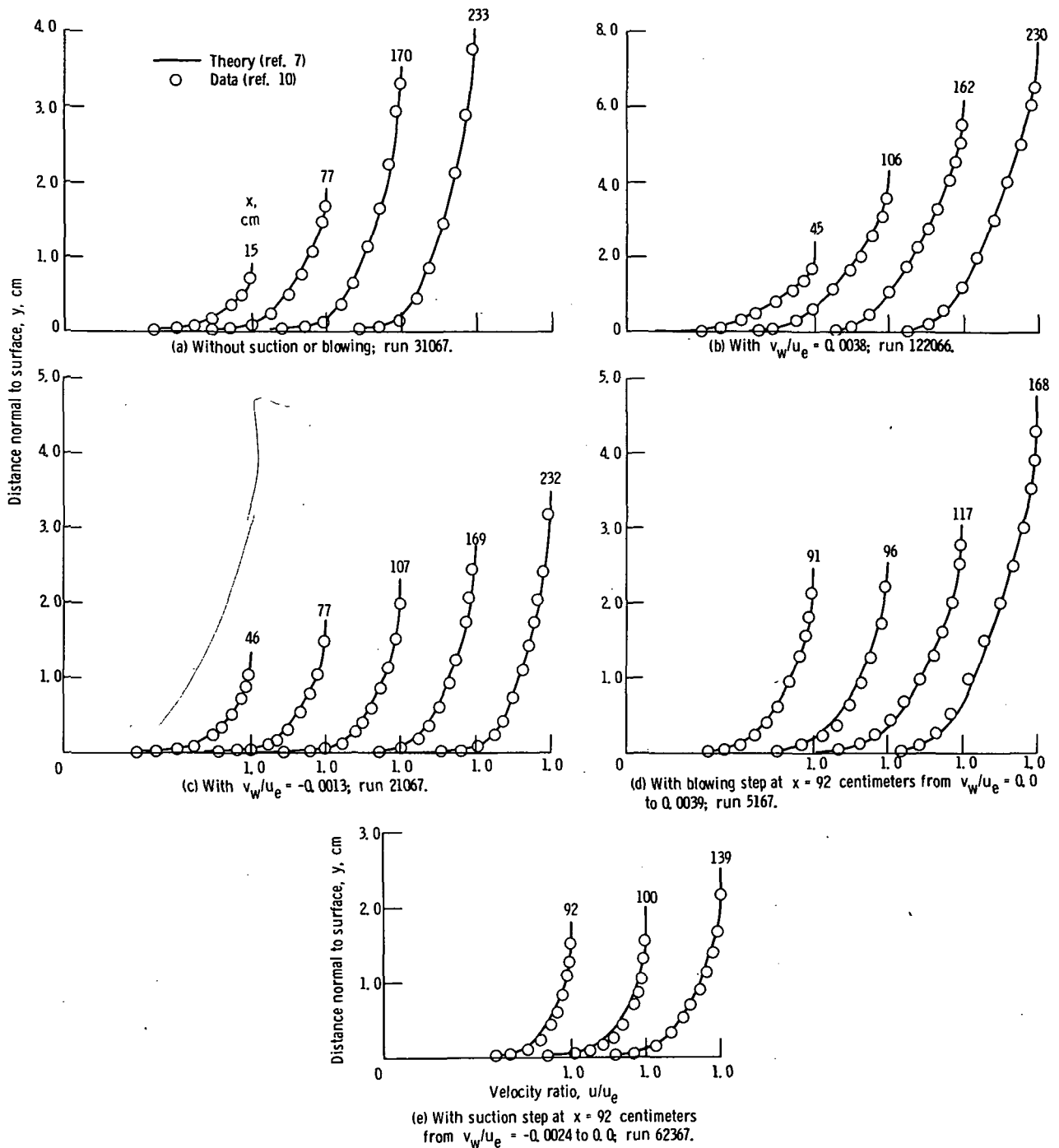| Theory (ref. 7) | Data (ref. 10) | Run | $v_w/u_e$ (upstream) | $v_w/u_e$ (downstream) |
|---|---|---|---|---|
| ——— | O | 31067 | 0.0 | 0.0 |
| – – – | □ | 42567 | .0 | .001 |
| –·–·– | ◇ | 5167 | .0 | .0039 |

| Theory (ref. 7) | Data (ref. 10) | Run | $v_w/u_e$ (upstream) | $v_w/u_e$ (downstream) |
|---|---|---|---|---|
| ——— | O | 31067 | 0.0 | 0.0 |
| – – – | □ | 62367 | -.0024 | .0 |

Skin friction coefficient, $C_f$

Momentum thickness, $\theta$, cm

Displacement thickness, $\delta^*$, cm

Distance along surface, cm

(e) For step in blowing at $x = 92$ centimeters.

(f) For step in suction at $x = 92$ centimeters.

Figure 2. - Concluded.

20

4.0

3.0

Theory (ref. 7)
○ Data (ref. 10)

2.0

x,
cm

1.0

15

233

170

77

0

(a) Without suction or blowing; run 31067.

8.0

6.0

4.0

230

162

106

2.0

45

0

(b) With $v_w/u_e$ = 0.0038; run 122066.

Distance normal to surface, y, cm

5.0

4.0

3.0

2.0

232

169

107

77

46

1.0

0        1.0      1.0      1.0      1.0      1.0

(c) With $v_w/u_e$ = -0.0013; run 21067.

5.0

4.0

168

3.0

117

2.0

91      96

1.0

0        1.0      1.0      1.0      1.0

(d) With blowing step at x = 92 centimeters from $v_w/u_e$ = 0.0
to 0.0039; run 5167.

Distance normal to surface, y, cm

3.0

139

2.0

92      100

1.0

0        1.0      1.0      1.0

Velocity ratio, $u/u_e$

(e) With suction step at x = 92 centimeters
from $v_w/u_e$ = -0.0024 to 0.0; run 62367.

Figure 3. - Theoretical and experimental velocity profiles for Simpson flat plates.

21
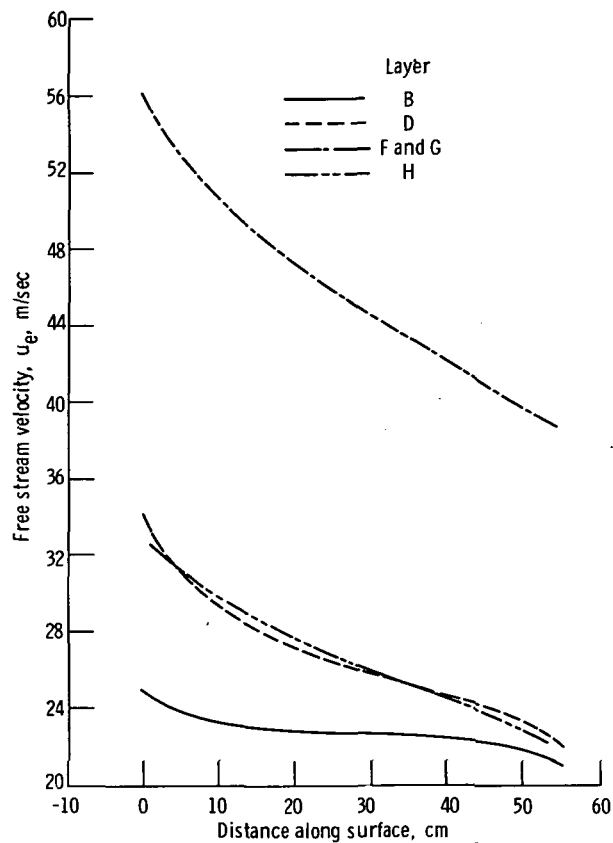
Figure 4. - Velocity distribution for Thompson airfoil (ref. 12).
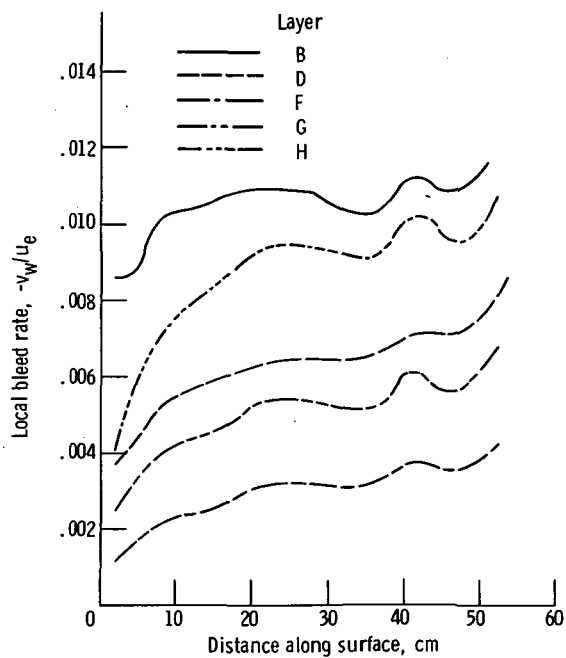


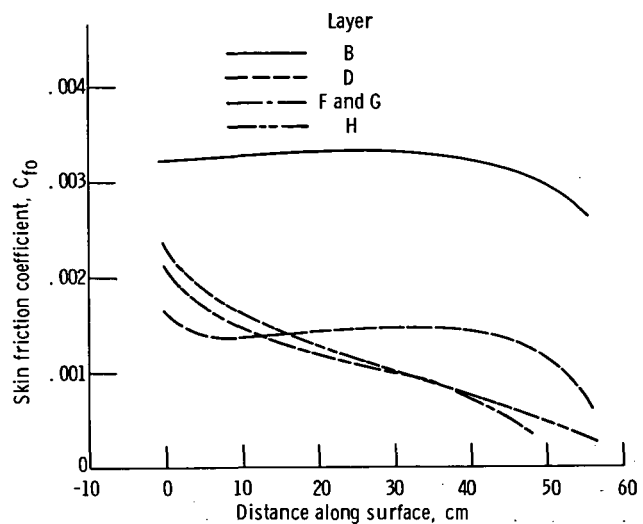Figure 5. - Bleed distribution for Thompson airfoil
(ref. 12).

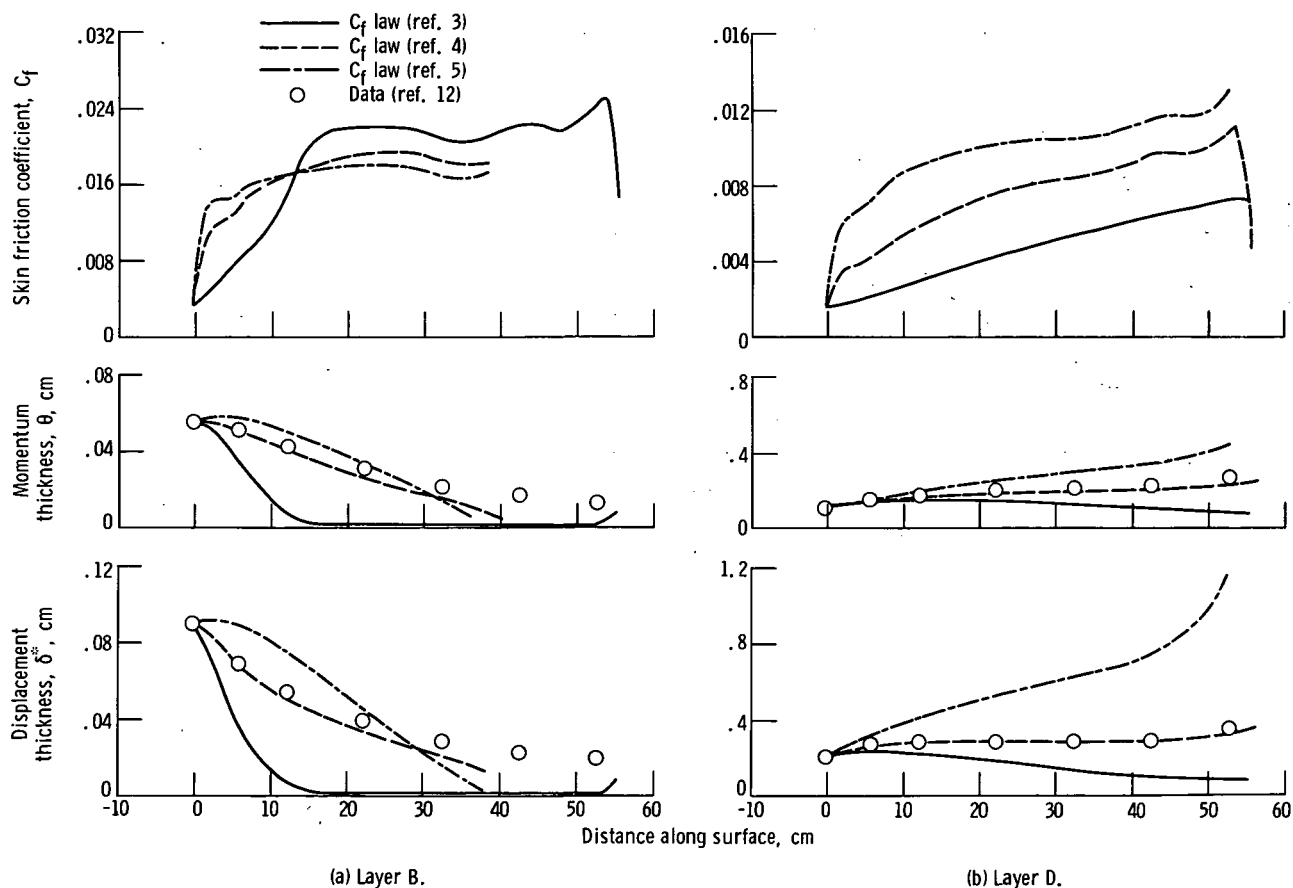Figure 6. – Theoretical skin friction coefficients on Thompson airfoil without bleed (ref. 3).



(a) Layer B.

(b) Layer D.

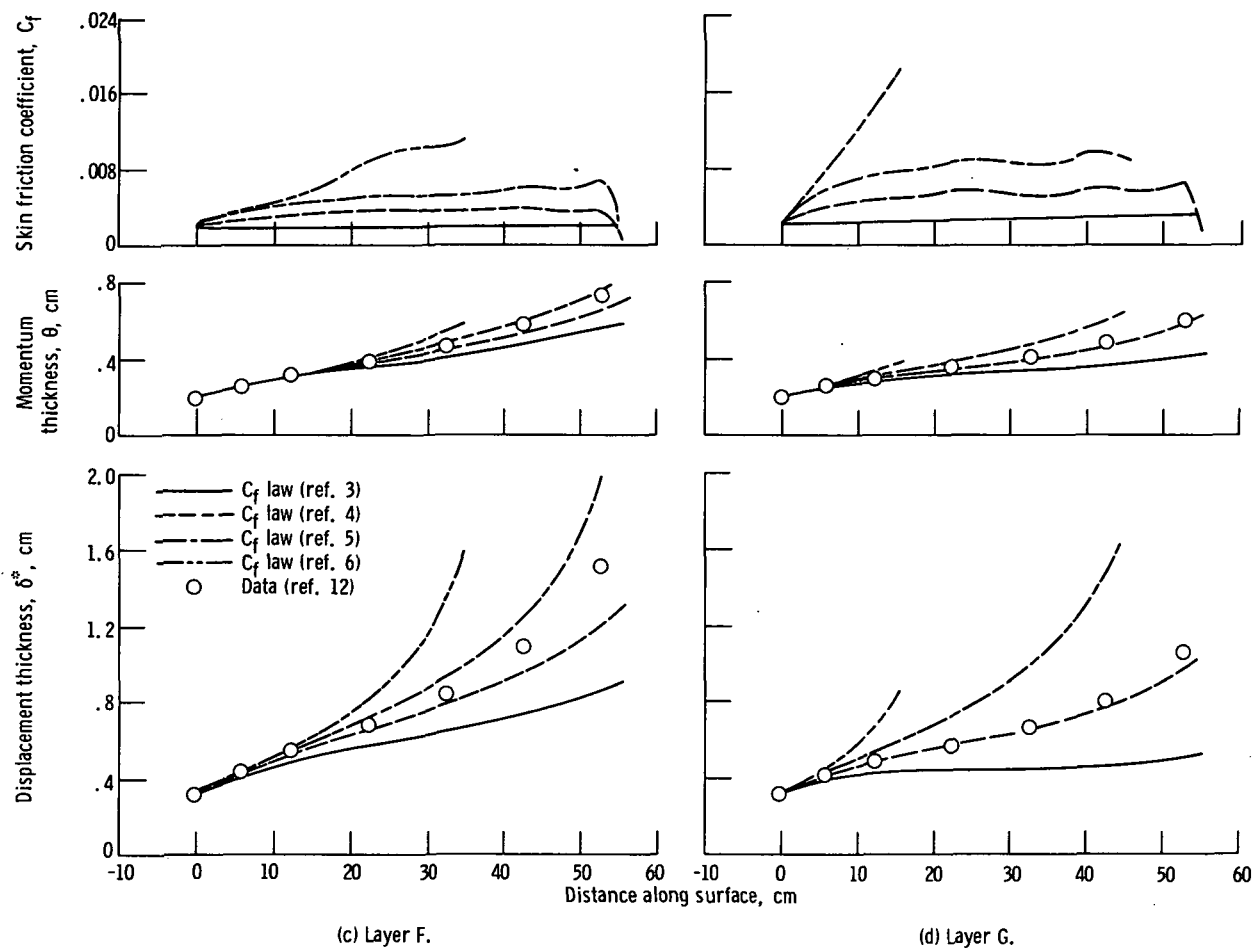Figure 7. – Effect of skin friction law on turbulent boundary layer analysis for Thompson airfoil.
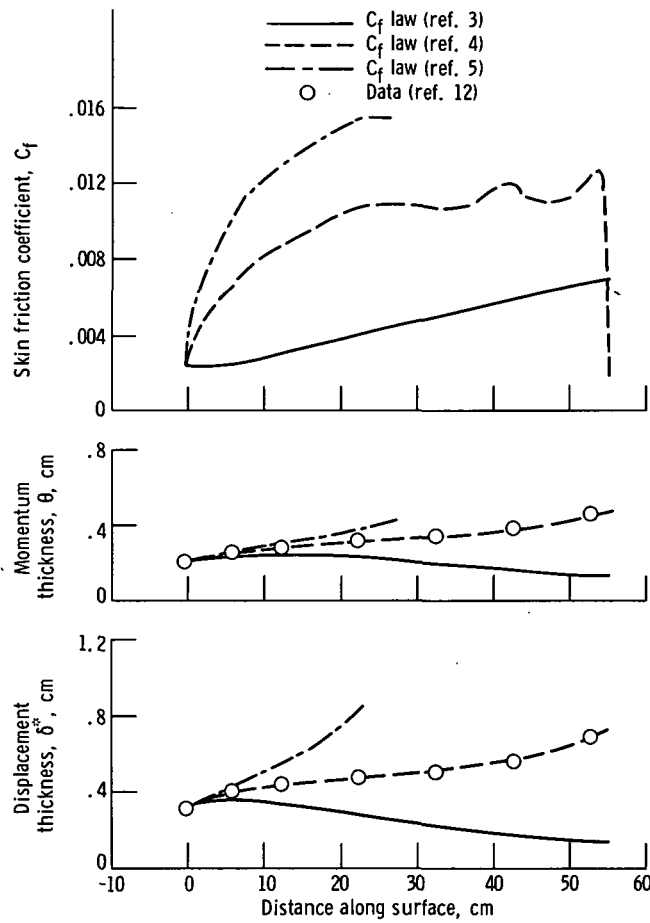
(c) Layer F.

(d) Layer G.

Figure 7. - Continued.

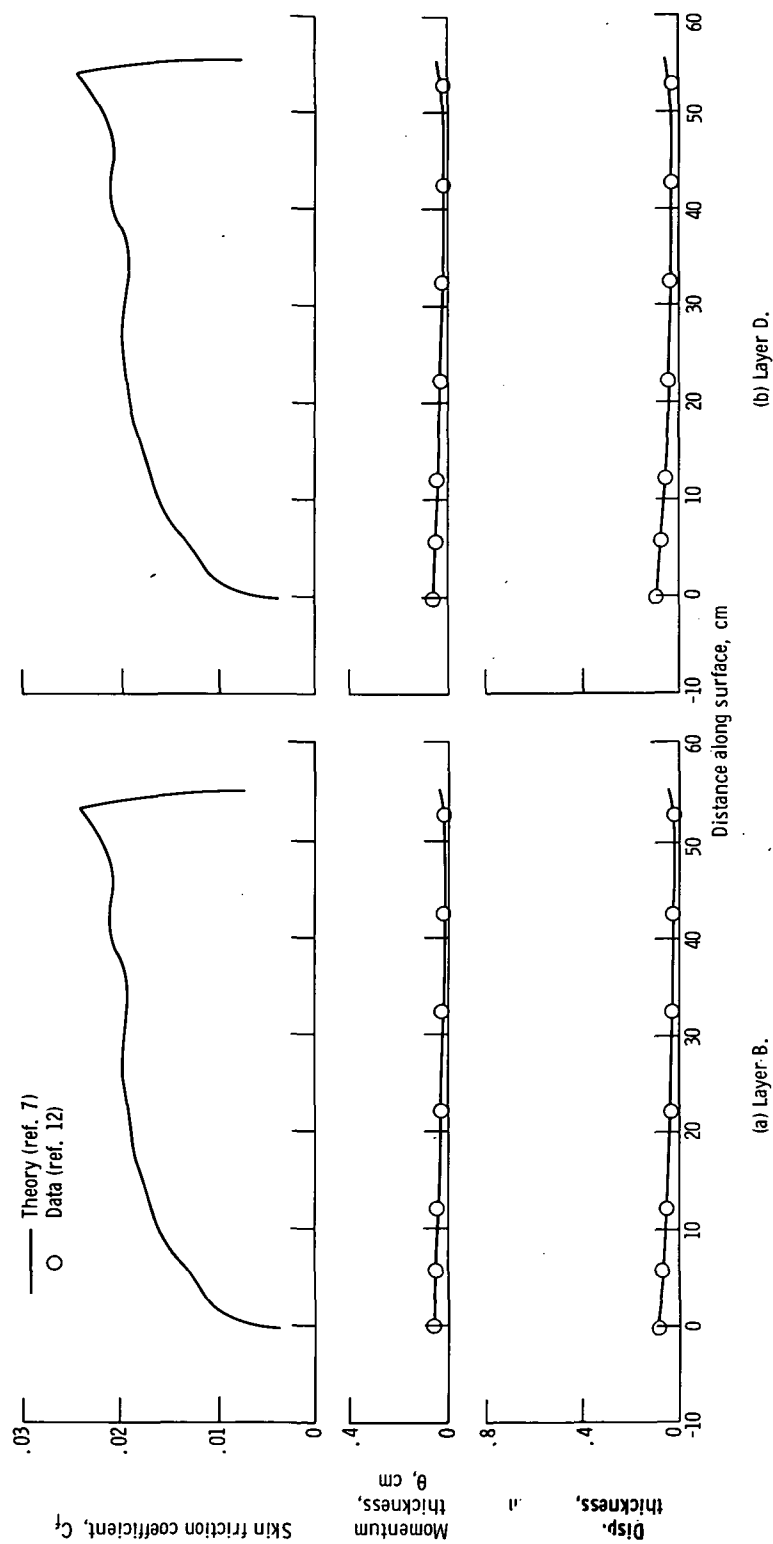(e) Layer H.

Figure 7. - Concluded.

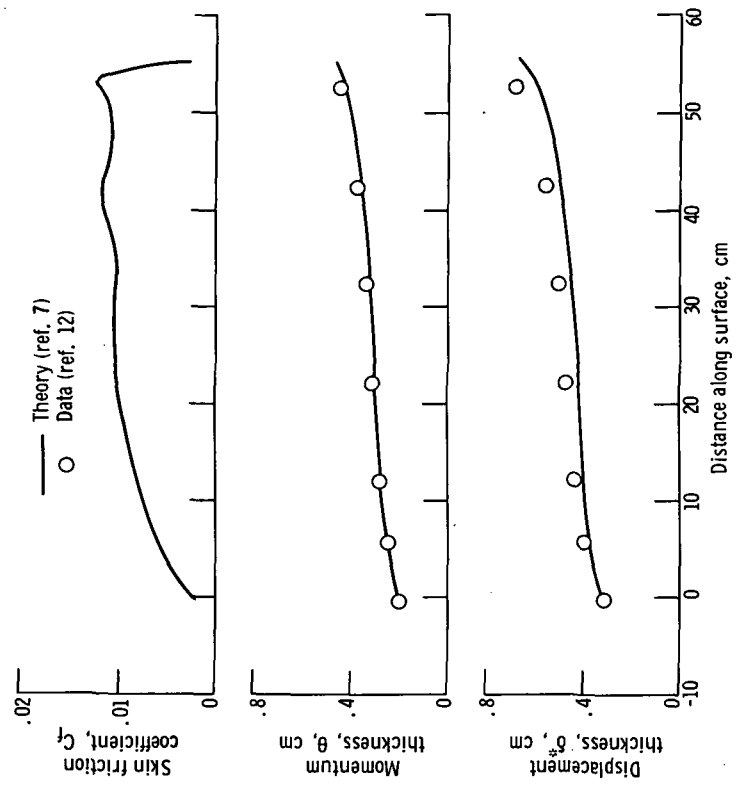Figure 8. - Theoretical and experimental results for Thompson airfoil.

(a) Layer B.

(b) Layer D.

(c) Layer F.

(d) Layer G.

Distance along surface, cm

Figure 8. - Continued.

Theory (ref. 7)
Data (ref. 12)

Skin friction coefficient, $C_f$

Momentum thickness, $\theta$, cm

Displacement thickness, $\delta^*$, cm

27

(e) Layer H.

Figure 8. – Concluded.
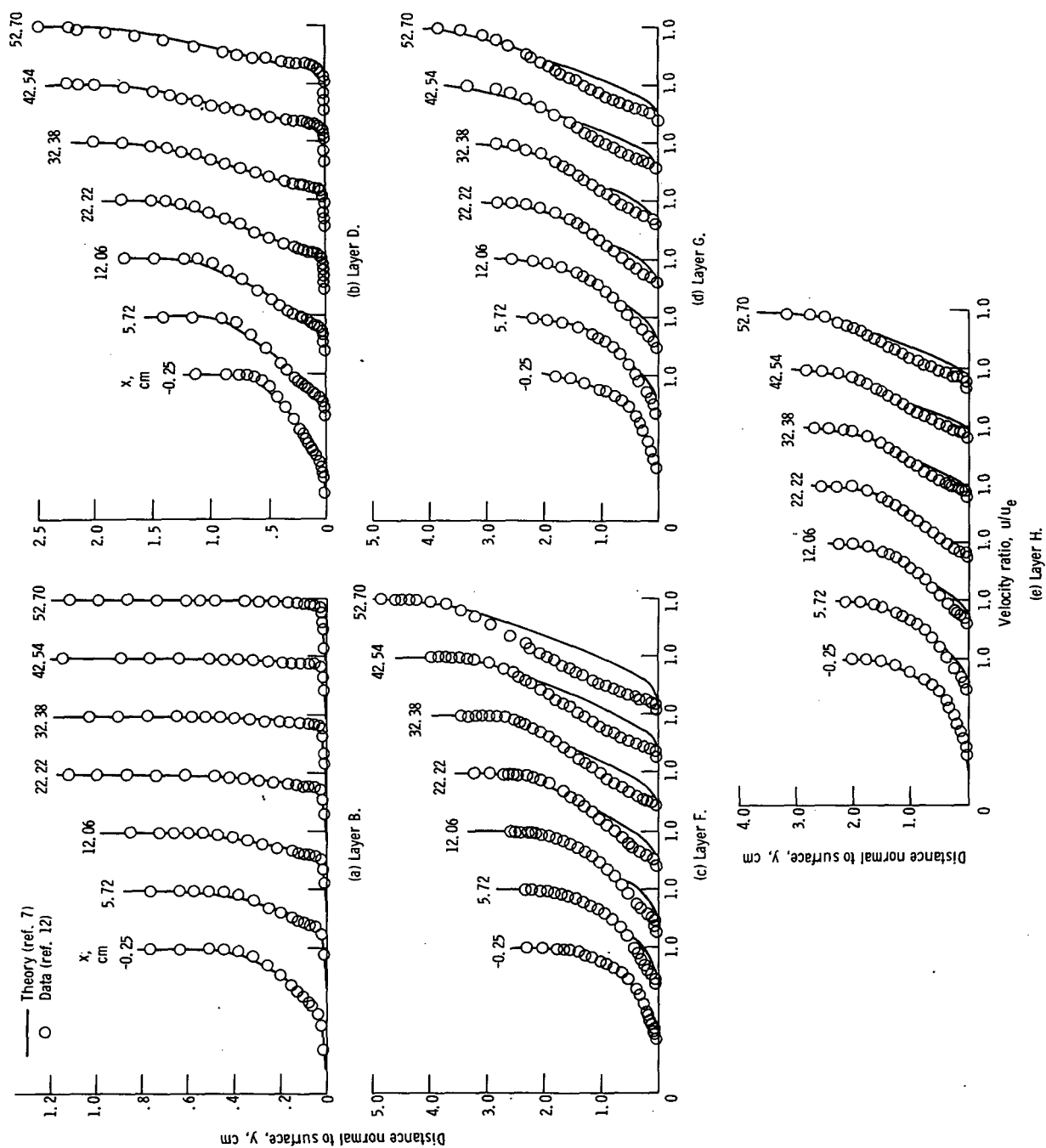
Figure 9. – Theoretical and experimental velocity profiles for Thompson airfoil.

29

(a) Distribution I.

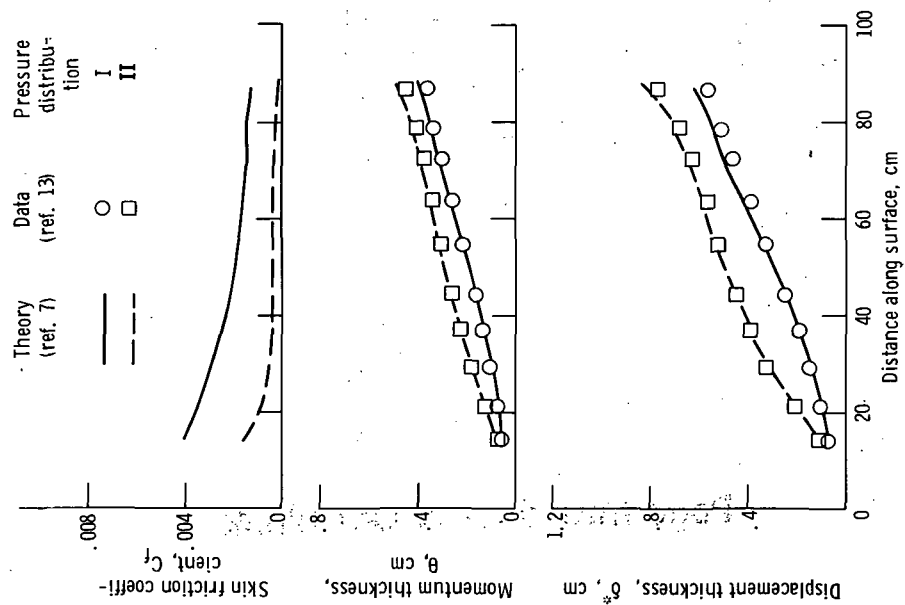(b) Distribution II.

Theory (ref. 7)
O Data (ref. 13)

$x$, cm

14.2  29.2  63.5  86.9

Velocity ratio, $u/u_e$

Distance normal to surface, $y$, cm

Figure 11. - Theoretical and experimental velocity profiles for McQuaid pressure distributions I and II.



| | Theory (ref. 7) | Data (ref. 13) | Pressure distribution |
|---|---|---|---|
| | —— | O | I |
| | – – | □ | II |

Skin friction coefficient, $C_f$

.008  .004  0

Momentum thickness, $\theta$, cm

.8  .4  0

Displacement thickness, $\delta^*$, cm
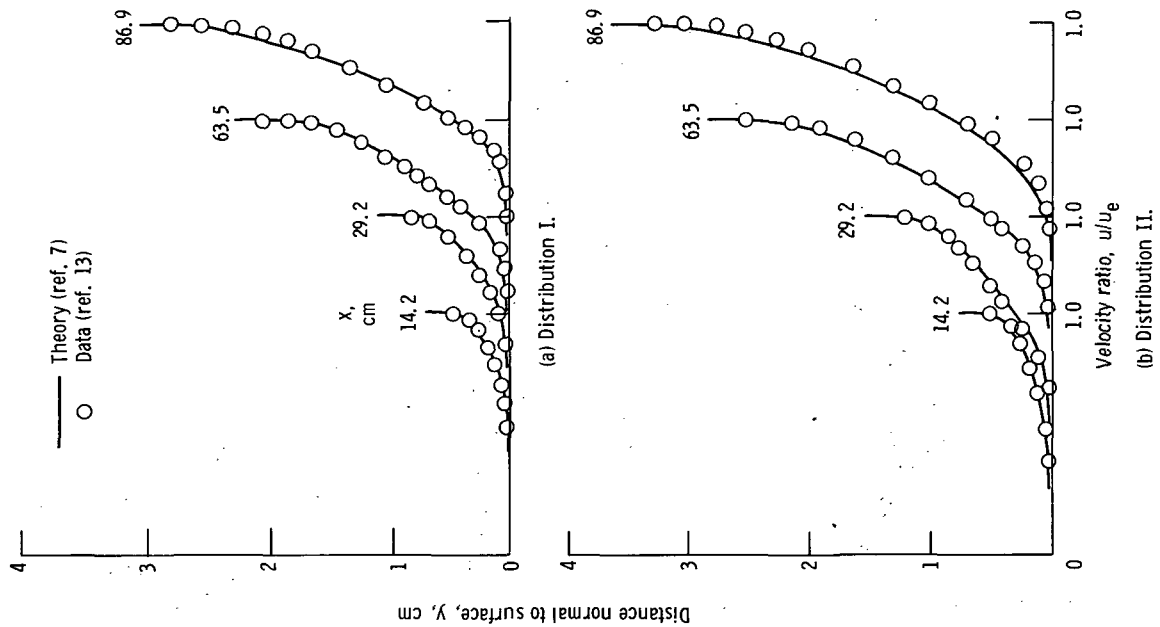
1.2  .8  .4  0

Distance along surface, cm

0  20  40  60  80  100

Figure 10. - Theoretical and experimental results for McQuaid pressure distributions I and II.

Page Intentionally Left Blank

*"The aeronautical and space activities of the United States shall be conducted so as to contribute . . . to the expansion of human knowledge of phenomena in the atmosphere and space. The Administration shall provide for the widest practicable and appropriate dissemination of information concerning its activities and the results thereof."*
—NATIONAL AERONAUTICS AND SPACE ACT OF 1958

# NASA SCIENTIFIC AND TECHNICAL PUBLICATIONS

TECHNICAL REPORTS: Scientific and technical information considered important, complete, and a lasting contribution to existing knowledge.

TECHNICAL NOTES: Information less broad in scope but nevertheless of importance as a contribution to existing knowledge.

TECHNICAL MEMORANDUMS: Information receiving limited distribution because of preliminary data, security classification, or other reasons. Also includes conference proceedings with either limited or unlimited distribution.

CONTRACTOR REPORTS: Scientific and technical information generated under a NASA contract or grant and considered an important contribution to existing knowledge.

TECHNICAL TRANSLATIONS: Information published in a foreign language considered to merit NASA distribution in English.

SPECIAL PUBLICATIONS: Information derived from or of value to NASA activities. Publications include final reports of major projects, monographs, data compilations, handbooks, sourcebooks, and special bibliographies.

TECHNOLOGY UTILIZATION PUBLICATIONS: Information on technology used by NASA that may be of particular interest in commercial and other non-aerospace applications. Publications include Tech Briefs, Technology Utilization Reports and Technology Surveys.

*Details on the availability of these publications may be obtained from:*

## SCIENTIFIC AND TECHNICAL INFORMATION OFFICE

# NATIONAL AERONAUTICS AND SPACE ADMINISTRATION
### Washington, D.C. 20546